Spectral signatures of vibronic coupling in trapped cold ionic Rydberg systems

Joseph W. P. Wilkinson,[1] Weibin Li,[2] and Igor Lesanovsky[1, 2]

[1] *Institut für Theoretische Physik, Universität Tübingen, Auf der Morgenstelle 14, 72076 Tübingen, Germany*

[2] *School of Physics and Astronomy and Centre for the Mathematics and Theoretical Physics of Quantum Non-Equilibrium Systems, The University of Nottingham, Nottingham, NG7 2RD, United Kingdom*

(Dated: April 24, 2024)

Atoms and ions confined with electric and optical fields form the basis of many current quantum simulation and computing platforms. When excited to high-lying Rydberg states, long-ranged dipole interactions emerge which strongly couple the electronic and vibrational degrees of freedom through state-dependent forces. This vibronic coupling and the ensuing hybridization of internal and external degrees of freedom manifest through clear signatures in the many-body spectrum. We illustrate this by considering the case of two trapped Rydberg ions, for which the interaction between the relative vibrations and Rydberg states realizes a quantum Rabi model. We proceed to demonstrate that the aforementioned hybridization can be probed by radio frequency spectroscopy and discuss observable spectral signatures at finite temperatures and for larger ion crystals.

Introduction.—Systems of trapped ions have led to a number of breakthroughs in the fields of quantum many-body and non-equilibrium physics [1–3]. They have been used to study quantum phases of interacting spins [4–6], quantum phase transitions in open quantum many-body systems [7–9], quantum thermodynamics principles [10], and molecular physics using Rydberg aggregates [11–13]. In conventional trapped ion quantum simulators, ions in energetically low-lying electronic states are employed to encode fictitious spin degrees of freedom (qubits) [14–18]. Interactions and high-fidelity conditional operations are then mediated using a so-called phonon bus [19, 20], the required spin-phonon or vibronic coupling being achieved by state-dependent light shifts [21]. In a relatively recent development (see, e.g., Refs. [22–27]), trapped ions have been excited to energetically high-lying electronic states, known as Rydberg states, that interact via electric dipole forces. This mechanism allows for the implementation of strong coherent interactions, which have been utilized to generate submicrosecond entangling gate operations [28], and to mediate effective spin interactions that do not rely on the phonon bus. It also frees up the phonon degrees of freedom, augmenting the trapped ion quantum simulator, facilitating the study of a range of interesting many-body phenomena in which trap vibrational modes are coupled to interacting electronic states [29–33].

In this work, we investigate a scenario where we create strong vibronic coupling in the electronic Rydberg state manifold between a pair of trapped ions. This is achieved by exciting Rydberg states under so-called facilitation or anti-blockade conditions [34–41]. Within this regime, the vibronic coupling between excited electronic states and phonons modes is described by a variant of the quantum Rabi model [42]. We show how the hybridized states can be experimentally probed via radio frequency modulation of the Rydberg state excitation laser, discuss the spectral signatures of the vibronic coupling, and also study their dependence on the temperature and number of ions. Our investigation highlights the potential in using systems of trapped ions, or even atoms, excited to Rydberg states to realize complex scenarios with coupled electronic and vibrational motion that are of the utmost importance in, e.g., biological processes [43], chemical reactions [44–46], and molecular dynamics [47–49].

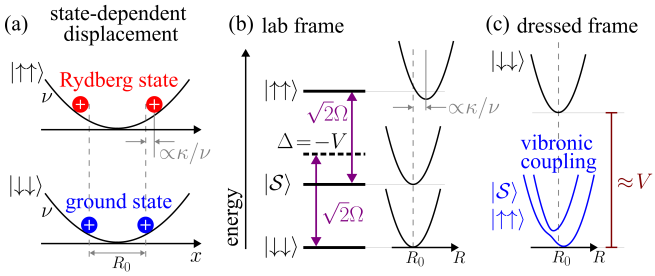

Figure 1. **System.** (a) Two ions confined within a harmonic potential with trap frequency ν. When both ions are in their electronic ground states, i.e., $|{\downarrow\downarrow}\rangle = |{\downarrow}\rangle \otimes |{\downarrow}\rangle$, the equilibrium distance between the ions is R_0. However, when both ions are simultaneously excited to Rydberg states $|{\uparrow\uparrow}\rangle$, electric dipole interactions displace the ions from their equilibrium positions by an amount proportional to κ/ν where κ parameterizes the strength of vibronic (i.e., spin-phonon) coupling. (b) Relevant energy levels for the system of trapped ions in the (stationary) lab frame. The laser, with detuning Δ and Rabi frequency Ω, couples the state $|{\downarrow\downarrow}\rangle$, via the singly-excited symmetric state $|\mathcal{S}\rangle = [|{\uparrow\downarrow}\rangle + |{\downarrow\uparrow}\rangle]/\sqrt{2}$, to the doubly-excited (Rydberg) state $|{\uparrow\uparrow}\rangle$. We consider the regime where the laser detuning cancels the interaction between the Rydberg ions at their equilibrium separation R_0 (i.e., $\Delta = -V$). Electric dipolar forces between the Rydberg ions couple the electronic and relative vibrational motion. (c) External dynamics in the (rotating) dressed frame of the laser. In the state $|{\downarrow\downarrow}\rangle$, the ions experience a virtually unperturbed confinement, however, in the states $|\mathcal{S}\rangle$ and $|{\uparrow\uparrow}\rangle$, they hybridize with the relative motional degrees of freedom. The resulting coupled electronic potential surfaces are located at an energy of approximately $E \approx -V$.

Model.—We consider a chain of ions trapped within a linear Paul trap. The internal degrees of freedom of each ion are modelled by two levels, denoted $|\downarrow\rangle$ and $|\uparrow\rangle$, that, respectively, represent an electronically low-lying ground state and high-lying excited Rydberg state of an alkaline earth metal ion [50]. These states are coupled by a laser with Rabi frequency Ω and detuning Δ. The state $|\uparrow\rangle$ is assumed to be a dressed Rydberg state that is generated by coupling two suitably chosen states from the Rydberg manifold via a microwave (MW) field (see Refs. [26–28]). This dressing technique produces strong and controllable electric dipole-dipole interactions amongst Rydberg ions with a strength parameterized by $V \propto d^2/R_0^3$ with d the electric transition dipole moment between the microwave coupled Rydberg states and R_0 the equilibrium distance between the ions [51]. The interaction amongst Rydberg states also gives rise to mechanical forces that, as shown in Fig. 1a, induce state-dependent displacements [31, 52]. Note that mechanical effects are also present when single trapped ions are excited into Rydberg states [25, 53]. For simplicity, we will not account for these here as they can be eliminated through precise control of the polarizability of the MW dressed Rydberg states [54].

To illustrate our ideas, we initially consider a system that consists of two ions, as depicted in Fig. 1a, and later generalize to many ions. For brevity, we only outline the derivation of the spin-phonon coupled Hamiltonian here, and reserve further relevant details to the Supplemental Material (SM) [51]. The model Hamiltonian for a system of trapped Rydberg ions is given by (n.b., $\hbar = 1$),

$$H = \sum_{i=1}^{2} h_i + V_{12} n_1 n_2 + \omega_2 a_2^\dagger a_2, \quad h_i = \Delta n_i + \Omega \sigma_i^x, \tag{1}$$

where $n_i = |\uparrow\rangle\langle\uparrow|_i$ is the projector onto the Rydberg state of ion i and $\sigma_i^x = |\uparrow\rangle\langle\downarrow|_i + |\downarrow\rangle\langle\uparrow|_i$ the associated spin-flip operator. The first two terms describe the effective spin dynamics modelling the ions' internal electronic degrees of freedom, the former the interactions of the ions with the electric field, and the latter the interactions between the ions in the Rydberg states via the distance-dependent potential $V_{12} = V(R_{12})$ with R_{12} the interionic distance. The final term governs the external vibrational degrees of freedom, which are modelled by a single phonon mode of frequency ω_2 with creation and annihilation operators $a_2^\dagger$ and a_2. In order to obtain a leading order coupling term, we linearly expand the dipole-dipole interaction potential $V(R_{12})$ about the equilibrium separation R_0 between the ions [33–35, 55]. Expressing the displacements of the ions about their equilibrium positions in terms of the phonon mode operators we get $V_{12} \approx V + \sum_{p=1}^{2} \kappa_p [a_p^\dagger + a_p]$ with the spin-phonon coupling strength given by,

$$\kappa_p = -\frac{3V}{R_0} \frac{\Gamma_p}{\sqrt{2M\omega_p}}, \quad V = \frac{1}{4\pi\epsilon_0} \frac{d^2}{R_0^3}. \tag{2}$$

Here, M is the ion mass and Γ_p the coupling coefficient associated to the phonon mode p with frequency ω_p. For two ions, state-dependent forces only couple the relative vibrational motion with the electronic dynamics. In terms of the ion trap frequency ν (see Fig. 1a), the frequency of the relative mode is $\omega_2 = \sqrt{3}\nu$ and the coupling strength $\kappa_2 < 0$ since $\Gamma_2 = \sqrt{2}$. In contrast, for the center of mass mode we have $\omega_1 = \nu$, yet $\kappa_1 = 0$ as $\Gamma_1 = 0$. Accordingly, the Hamiltonian reads (see Eq. (S61) in the SM [51]),

$$H = \sum_{i=1}^{2} h_i + V n_1 n_2 + \omega_2 a_2^\dagger a_2 + \kappa_2 [a_2^\dagger + a_2] n_1 n_2. \tag{3}$$

The strength of the spin-phonon coupling κ_p scales as $\kappa_p \sim M^{5/6} \nu^{13/6}$, therefore, the heavier the ion and larger the trap frequency, the stronger the coupling between the electronic and vibrational motion [51]. For two ions, this is why we consider barium $^{138}\mathrm{Ba}^+$ ions of isotopic mass $M = 137.9\,\mathrm{u}$ as opposed to strontium $^{88}\mathrm{Sr}^+$ ($M = 87.9\,\mathrm{u}$) or calcium $^{40}\mathrm{Ca}^+$ ($M = 40.0\,\mathrm{u}$) ions which are currently used in trapped Rydberg ion experiments [26]. Here, the electronically low-lying ground state $|\downarrow\rangle$ is the metastable state $|5\mathrm{D}_{5/2}\rangle$, whilst the highly-excited dressed Rydberg state $|\uparrow\rangle$ is a superposition $|\uparrow\rangle = [|n\mathrm{P}_{1/2}\rangle - |n\mathrm{S}_{1/2}\rangle]/\sqrt{2}$. These two states are coupled by a two-photon excitation scheme via the intermediate state $|7\mathrm{P}_{3/2}\rangle$ [26, 28]. Using Rydberg states with a principal quantum number $n = 60$ and linear Paul trap with frequency $\nu = 2\pi \times 6\,\mathrm{MHz}$, we obtain an equilibrium ion separation $R_0 = 1.12\,\mu\mathrm{m}$ which returns an interaction strength $V = 28\omega_2$ and a coupling strength $\kappa_2 = -0.20\omega_2$ (see Fig. 2b). We note that these values are somewhat extreme, yet feasible [26]. Later, we will show that these can be relaxed significantly to more typical values when considering larger ion crystals.

Spectrum.—In the following, we consider the situation in which the dynamics is subject to the facilitation (anti-blockade) constraint where the laser detuning Δ cancels the interaction energy V (i.e., $\Delta + V = 0$), as illustrated in Fig. 1b. In this regime, the spin-phonon coupling is particularly prominent and a simplified analytical model can be developed. Due to the level symmetry, the laser only couples the unexcited state $|\downarrow\downarrow\rangle$, the singly-excited symmetric state $|\mathcal{S}\rangle = [|\uparrow\downarrow\rangle + |\downarrow\uparrow\rangle]/\sqrt{2}$, and the doubly-excited Rydberg state $|\uparrow\uparrow\rangle$ (see Fig. 1b), with the singly-excited antisymmetric state $|\mathcal{A}\rangle = [|\downarrow\uparrow\rangle - |\uparrow\downarrow\rangle]/\sqrt{2}$ decoupled from the aforementioned dynamics. Taking into account that the interaction energy $V \gg \Omega$, we note that the state $|\downarrow\downarrow\rangle$ only acquires a weak light shift and so can similarly be neglected. On the other hand, the states $|\mathcal{S}\rangle$ and $|\uparrow\uparrow\rangle$ are resonantly coupled to the laser field with the electronic state $|\uparrow\uparrow\rangle$ also coupled to the vibrational mode. The approximate Hamiltonian is then (see SM [51]),

$$H = \begin{bmatrix} -V & \sqrt{2}\Omega \\ \sqrt{2}\Omega & -V \end{bmatrix} + \omega_2 a_2^\dagger a_2 + \kappa_2 \begin{bmatrix} 1 & 0 \\ 0 & 0 \end{bmatrix} [a_2^\dagger + a_2], \tag{4}$$

where the energy of the hybridized states is with respect to the state $|\downarrow\downarrow\rangle$, as pictured in Fig. 1c.

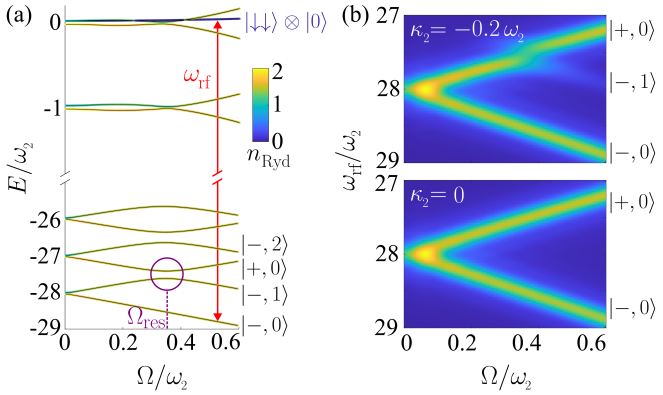

Figure 2. **Spectrum and radio frequency spectroscopy.** (a) Energy spectrum of the two-ion Hamiltonian in Eq. (3) for $V = -\Delta = 28\omega_2$ with $\kappa_2 = -0.20\omega_2$ as a function of the Rabi frequency Ω. The color of the line encodes the average number of Rydberg excitations $n_{\rm Ryd} = \langle n_1 + n_2 \rangle$ of the approximate eigenstate. The blue line represents the initial state $|\downarrow\downarrow\rangle \otimes |0\rangle$ which is adiabatically connected to the electronic state $|\downarrow\downarrow\rangle$ in the limit $\kappa_2 \to 0$ since, for all Ω considered, it contains only a tiny admixture of the Rydberg states $|\uparrow\rangle$. Transitions between states are driven by applying a radio frequency (rf) field with frequency $\omega_{\rm rf}$. This facilitates the probing of the coupling that occurs in the vicinity of the resonance at $\Omega = \Omega_{\rm res} = \omega_2/2\sqrt{2}$, marked by the purple circle. Note that the states in the lower branches denote eigenstates in the limit $\kappa_2 \to 0$ (see the main text for details). (b) Spectroscopy of the hybridized electronic and vibrational states. The system is initially prepared in the state $|\downarrow\downarrow\rangle \otimes |0\rangle$ for fixed Ω. Irradiating the ions with an rf field of frequency $\omega_{\rm rf}$ with strength $\Omega_{\rm rf} = 0.1\omega_2$ (cf. Eq. (7)) and integrating the average number of Rydberg excitations over a period $\omega_2 \tau = 30$ yields the signal shown. In the upper panel, where $\kappa_2 = -0.20\omega_2$, the hybridization clearly manifests as an avoided crossing. This is in contrast to the lower panel, where $\kappa_2 = 0$, and the electronic and vibrational motion decouple.

In Fig. 2a, we show the full vibronic coupled spectrum for $V = 28\omega_2$ and $\kappa_2 = -0.20\omega_2$ as a function of the laser Rabi frequency Ω. In the region with energy $E \approx -V$, we indeed observe an avoided crossing, indicated by a circle, which is a manifestation of the strong coupling between the internal electronic and external vibrational degrees of freedom. In order to study this coupling, we remark that the interaction strength $V \gg \kappa_2$ which allows us to treat the spin-phonon coupling as a perturbation. Introducing the following electronic eigenstates $|\pm\rangle = [|\uparrow\uparrow\rangle \pm |\mathcal{S}\rangle]/\sqrt{2}$ of the unperturbed Hamiltonian (i.e., for $\kappa_2 = 0$), we can then rewrite the approximate model Hamiltonian as,

$$H = \begin{bmatrix} E_+ & 0 \\ 0 & E_- \end{bmatrix} + \omega_2 a_2^\dagger a_2 + \frac{\kappa_2}{2} \begin{bmatrix} 1 & 1 \\ 1 & 1 \end{bmatrix} [a_2^\dagger + a_2], \qquad (5)$$

with $E_\pm = -V \pm \sqrt{2}\Omega$ the electronic energy eigenvalues. This Hamiltonian is a variant of the quantum Rabi model with spin-phonon coupling constant κ_2 [42]. For $\kappa_2 = 0$, the spin-phonon dynamics decouple and the Hamiltonian becomes diagonal. The corresponding energy eigenvalues

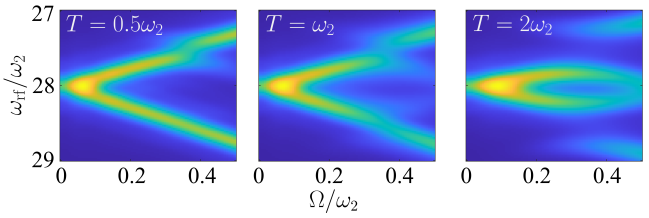

Figure 3. **Spectroscopy at finite temperature.** Radio frequency spectra for the initially prepared state $|\downarrow\downarrow\rangle\langle\downarrow\downarrow| \otimes \rho_T$ at different temperatures T. Initial states with high vibrational mode quantum numbers n couple to more symmetric parts of the spectrum. As such, the higher the temperature, the more symmetric the signal becomes about $\omega_{\rm rf} = V$. The data plotted is generated using the parameters given in Fig. 2 with the coupling strength $\kappa_2 = -0.20\omega_2$ (see Fig. 2b for details). Note that for $\kappa_2 = 0$, all these plots would be indistinguishable from the bottom panel of Fig. 2b.

are $E_{\pm,N} = E_\pm + N\omega_2$, whilst the associated eigenstates are $|\pm, N\rangle = |\pm\rangle \otimes |N\rangle$, where $|N\rangle$ is an eigenstate of the number operator with eigenvalue N. A resonance occurs when any pair of these energies becomes degenerate, e.g., the resonance shown in Fig. 2a is due to states $|+,0\rangle$ and $|-,1\rangle$, which become degenerate at $\Omega = \Omega_{\rm res} \approx \omega_2/2\sqrt{2}$. Notice that this is only an estimate for the value of the resonance frequency $\Omega_{\rm res}$, since we are neglecting second order light shifts. In general, resonances occur whenever the Rabi frequency $\Omega = \Omega_{\rm res} \approx N\omega_2/2\sqrt{2}$ with $N \in \mathbb{N}$. If we calculate the approximate eigenstates at the resonance between the states $|+,0\rangle$ and $|-,1\rangle$ highlighted in Fig. 2a, we find that [51],

$$|E_\pm^{\rm res}\rangle = \frac{1}{2}\big[|\uparrow\uparrow\rangle \otimes [|1\rangle \pm |0\rangle] - |\mathcal{S}\rangle \otimes [|1\rangle \mp |0\rangle]\big], \qquad (6)$$

which evidently shows hybridization of the electronic and vibrational degrees of freedom. The resonant energy level splitting is given by the coupling strength κ_2.

Spectroscopy.—In order to probe the energy spectrum shown in Fig. 2a in an experiment, we propose to perform radio frequency (rf) spectroscopy. To implement this, we replace the Rabi frequency in Eq. (3) according to,

$$\Omega \to \Omega(t) = \Omega + \Omega_{\rm rf} \cos(\omega_{\rm rf} t), \qquad (7)$$

where $\omega_{\rm rf}$ and $\Omega_{\rm rf}$ are the radio frequency and amplitude modulation of the field. The spectroscopic protocol is as follows. To start, we prepare the system in the unexcited state $|\downarrow\downarrow\rangle \otimes |0\rangle$, i.e., the state within which both the spins and the phonon are, respectively, in their electronic and vibrational ground states. Next, we switch on the laser to set the desired value for the time-independent part of the Rabi frequency (i.e., $\Omega \neq 0$ and $\Omega_{\rm rf} = 0$). Assuming that this proceeds adiabatically, this amounts to moving along the blue line in Fig. 2a. Note, however, that in practice, a sudden turning on of the laser should also suffice, since for all considered values of the Rabi frequency the state

colored in blue corresponds to the initial state $|\downarrow\downarrow\rangle \otimes |0\rangle$, up to corrections of order $[\Omega/V]^2$. Now the rf modulation is switched on (i.e., $\Omega_{\rm rf} \neq 0$) and, if the radio frequency $\omega_{\rm rf}$ is set to the energy splitting between two hybridized levels, illustrated by the red arrow in Fig. 2a, a transition occurs. Given that the initial state contains no Rydberg excitations, monitoring the number of ions that are in Rydberg states provides a direct spectroscopic signature of whether a transition has taken place, as demonstrated in Fig. 2b, where we plot the time-integrated number of Rydberg excitations $I = \int_0^\tau {\rm d}t\, \langle n_1 + n_2\rangle(t)$ as a function of $\omega_{\rm rf}$ and $\Omega(t)$ over the time interval $\omega_2 \tau = 30$.

Transitions can only occur if the Hamiltonian possesses a non-vanishing matrix element between initial and final states. For the chosen initial state $|\downarrow\downarrow\rangle \otimes |0\rangle$, this is only the case if the final state contains some admixture of the state $|\mathcal{S}\rangle \otimes |0\rangle$. Hence, in the limit $\kappa_2 = 0$, only the states $|\pm, 0\rangle$ can be excited, as demonstrated in the lower panel of Fig. 2b. However, with increased vibronic coupling the electronic and vibrational motion hybridize such that, in the vicinity of the resonance denoted in Fig. 2a, the state is approximated by that in Eq. (6). Given that this state exhibits overlap with the state $|\mathcal{S}\rangle \otimes |0\rangle$, it can be excited from the initial state and, from inspection of Fig. 2b, one clearly observes the associated avoided crossing.

At finite temperature, the initial phonon state is a thermal state, $\rho_T = \sum_{N=0}^{\infty} {\rm e}^{-N\omega_2/T}/[1-{\rm e}^{-\omega_2/T}]|N\rangle\langle N|$. The occupation of these higher vibrational states opens novel transition channels. Indeed, in contrast to the case where $T = 0$, these aforementioned transitions do not probe the lower edge of the spectrum, delimited by the state $|-, 0\rangle$ (see Fig. 2b), whose energy decreases linearly with Ω. Rather, they lead to states being symmetrically repelled by other states of higher and lower energy. For example, the initial state in Fig. 2a couples to states with asymptotes $|+, 0\rangle$ and $|-, 2\rangle$. This coupling to more symmetric parts of the spectrum manifests in a spectroscopic signal, as pictured in Fig. 3. For sufficiently low T, the signal is similar to that in the upper panel in Fig. 2b. However, as the temperature increases the signal becomes symmetric about $\omega_{\rm rf} = V$. Note that without spin-phonon coupling, the spectrum would be identical to that in the lower panel of Fig. 2b for all T. Hence, small, but finite temperatures increase the spectral signature of the vibronic coupling.

Ion crystals.—We now generalize our considerations to a chain of N ions confined within a linear Paul trap [27]. For simplicity, we assume that only the centermost pair of ions are irradiated with the laser such that the internal electronic degrees of freedom of the unexcited ions decouple from the many-body spin-phonon coupled dynamics. This leads to the following Hamiltonian [51],

$$H = \sum_{i=1}^{2} h_i + V n_1 n_2 + \sum_{p=1}^{N} [\omega_p a_p^\dagger a_p + \kappa_p [a_p^\dagger + a_p] n_1 n_2], \tag{8}$$

with the former two terms corresponding to the electronic motion defined as in Eq. (3) and where for simplicity the centermost pair of ions are labelled by $i = 1, 2$. The latter terms then respectively describe the external and coupled motion, with ω_p the frequency of the phonon mode p and κ_p the associated strength of the coupling to the internal dynamics. Note, for even numbers of ions N, the coupling coefficients Γ_p and, consequently, the coupling strengths κ_p [see Eq. (2)] for modes with odd p vanish. Hence, the corresponding modes decouple and can be neglected.

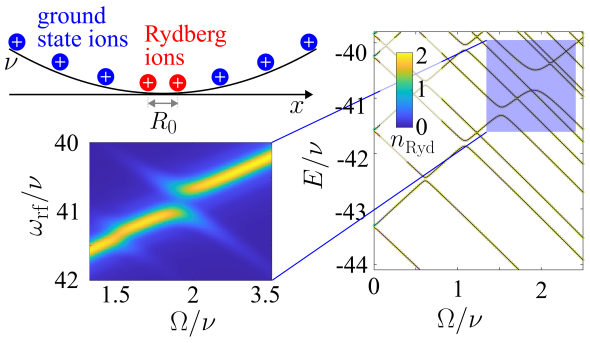

Figure 4. **Larger ion crystals.** Energy and radio frequency spectrum of a chain of trapped Rydberg ions. As the number of ions in the crystal N increases, the equilibrium separation between the two centermost ions R_0 decreases [56]. Here, we consider a chain of $N = 8$ strontium $^{88}{\rm Sr}^+$ ions confined in a trap with frequency $\nu = 2\pi \times 2\,{\rm MHz}$. In the electronic ground state $|\downarrow \cdots \downarrow\rangle$, the equilibrium separation between the central ions $R_0 = 1.37\,\mu{\rm m}$. When the centermost ions are excited to the Rydberg states $|\uparrow\rangle$, they interact with strength $V = 43\nu$. In contrast to the case of two ions (cf. Fig. 2), the two spins couple to four phonons of frequency $\omega_2 = 1.73\nu$, $\omega_4 = 3.06\nu$, $\omega_6 = 4.29\nu$, $\omega_8 = 5.44\nu$ with coupling strength $\kappa_2 = -0.06\nu$, $\kappa_4 = -0.10\nu$, $\kappa_6 = -0.15\nu$, $\kappa_8 = -0.27\nu$. Note, in particular, the coupling to the latter mode which manifests as an avoided crossing that can be probed via radio frequency spectroscopy (cf. Fig. 2b), as demonstrated in the outset.

Larger ion crystals give rise to increased spin-phonon coupling strengths since ions in the trap center get closer and their interaction features stronger forces (see Fig. 4). To demonstrate this we consider an ion crystal of $N = 8$ strontium $^{88}{\rm Sr}^+$ ions of mass $M = 87.9\,{\rm u}$ with parameter values that are significantly relaxed compared to the case of $N = 2$ barium $^{138}{\rm Ba}^+$ ions considered initially. Here, the state $|\downarrow\rangle = |4{\rm D}_{5/2}\rangle$ is a metastable state, whilst the state $|\uparrow\rangle = [|n{\rm P}_{1/2}\rangle - |n{\rm S}_{1/2}\rangle]/\sqrt{2}$ is a (dressed) Rydberg state with principal quantum number $n = 50$. With trap frequency $\nu = 2\pi \times 2\,{\rm MHz}$, the equilibrium separation of the centermost ions $R_0 = 1.37\,\mu{\rm m}$ and the corresponding interaction strength $V = 43\nu$. In contrast to the two ion case (see Fig. 1a), the spins now couple to four phonons, with frequencies and coupling strengths that are listed in Fig. 4. Here, the coupling to the $p = 8$ mode manifests in Fig. 4 as a clearly observable avoided crossing. Note that all parameters used are tabulated in the SM [51].

Summary and outlook.—In this work, we demonstrate

that strong state-dependent forces in Rydberg ions allow for the engineering and exploring of vibronic interactions in trapped ion quantum simulators. Spectral signatures of coupling between the electronic and vibrational motion are directly visible in the spectroscopy of Rydberg states with radio frequency modulated laser. Whilst we focused on analytically and numerically tractable situations, the exponential growth of the number of degrees of freedom rapidly allows one to reach many-body scenarios that are intractable on classical computers. Spatially resolved and quantitative Rydberg state spectroscopy in the precisely controllable environment of such augmented trapped ion quantum simulation platforms can be used to benchmark and advance numerical approximations schemes, e.g., by facilitating an understanding of which quantum correlations are most important to capture the observed spectral signatures as the number of degrees of freedom grows.

We gratefully acknowledge discussions with M. Hennrich. We are grateful for funding from the Deutsche Forschungsgemeinschaft (DFG, German Research Foundation) under Projects No. 428276754 and 435696605 as well as through the Research Unit FOR 5413/1, Grant No. 465199066. This project has also received funding from the European Union's Horizon Europe research and innovation program under Grant Agreement No. 101046968 (BRISQ). This work was supported by the University of Nottingham and the University of Tübingen's funding as part of the Excellence Strategy of the German Federal and State Governments, in close collaboration with the University of Nottingham. This work also received supported from the Engineering and Physical Sciences Research Council [grant numbers EP/V031201/1 and EP/W015641/1]. JW was supported by the University of Tübingen through a Research@Tübingen fellowship. The code used to produce the data supporting the findings of this article is available on Zenodo [57].

[1] M. Lewenstein, A. Sanpera, V. Ahufinger, B. Damski, A. Sen(De), and U. Sen, Ultracold atomic gases in optical lattices: mimicking condensed matter physics and beyond, Adv. Phys. **56**, 243 (2007).
[2] C. Gross and I. Bloch, Quantum simulations with ultracold atoms in optical lattices, Science **357**, 995 (2017).
[3] C. Monroe, W. C. Campbell, L.-M. Duan, Z.-X. Gong, A. V. Gorshkov, P. W. Hess, R. Islam, K. Kim, N. M. Linke, G. Pagano, P. Richerme, C. Senko, and N. Y. Yao, Programmable quantum simulations of spin systems with trapped ions, Rev. Mod. Phys. **93**, 025001 (2021).
[4] D. Porras and J. I. Cirac, Effective quantum spin systems with trapped ions, Phys. Rev. Lett. **92**, 207901 (2004).
[5] A. Friedenauer, H. Schmitz, J. T. Glueckert, D. Porras, and T. Schaetz, Simulating a quantum magnet with trapped ions, Nature Phys. **4**, 757 (2008).
[6] P. Schauß, J. Zeiher, T. Fukuhara, S. Hild, M. Cheneau, T. Macrì, T. Pohl, I. Bloch, and C. Gross, Crystallization in Ising quantum magnets, Science **347**, 1455 (2015).
[7] M. Greiner, M. Olaf, E. Tilman, T. W. Hänsch, and I. Bloch, Quantum phase transition from a superfluid to a Mott insulator in a gas of ultracold atoms, Nature **415**, 39 (2002).
[8] M. Vojta, Quantum phase transitions, Rep. Prog. Phys. **66**, 2069 (2003).
[9] S. Diehl, A. Micheli, A. Kantian, B. Kraus, H. P. Büchler, and P. Zoller, Quantum states and phases in driven open quantum systems with cold atoms, Nature Phys. **4**, 878 (2008).
[10] O. Abah, J. Roßnagel, G. Jacob, S. Deffner, F. Schmidt-Kaler, K. Singer, and E. Lutz, Single-ion heat engine at maximum power, Phys. Rev. Lett. **109**, 203006 (2012).
[11] S. Wüster, A. Eisfeld, and J. M. Rost, Conical intersections in an ultracold gas, Phys. Rev. Lett. **106**, 153002 (2011).
[12] D. W. Schönleber, A. Eisfeld, M. Genkin, S. Whitlock, and S. Wüster, Quantum simulation of energy transport with embedded Rydberg aggregates, Phys. Rev. Lett. **114**, 123005 (2015).
[13] S. Wüster, Quantum Zeno suppression of intramolecular forces, Phys. Rev. Lett. **119**, 013001 (2017).
[14] K. Kim, M.-S. Chang, R. Islam, S. Korenblit, L.-M. Duan, and C. Monroe, Entanglement and tunable spin-spin couplings between trapped ions Using multiple transverse modes, Phys. Rev. Lett. **103**, 120502 (2009).
[15] K. Kim, M.-S. Chang, S. Korenblit, R. Islam, E. E. Edwards, J. K. Freericks, G.-D. Lin, L.-M. Duan, and C. Monroe, Quantum simulation of frustrated Ising spins with trapped ions, Nature **465**, 590 (2010).
[16] J. T. Barreiro, M. Müller, P. Schindler, D. Nigg, T. Monz, M. Chwalla, M. Hennrich, C. F. Roos, P. Zoller, and R. Blatt, An open-system quantum simulator with trapped ions, Nature **470**, 486 (2011).
[17] M. Müller, K. Hammerer, Y. L. Zhou, C. F. Roos, and P. Zoller, Simulating open quantum systems: from many-body interactions to stabilizer pumping, New J. Phys. **13**, 085007 (2011).
[18] C. Schneider, D. Porras, and T. Schaetz, Experimental quantum simulations of many-body physics with trapped ions, Rep. Prog. Phys. **75**, 024401 (2012).
[19] C. D. Bruzewicz, J. Chiaverini, R. McConnell, and J. M. Sage, Trapped-ion quantum computing: progress and challenges, Appl. Phys. Rev. **6**, 021314 (2019).
[20] T. Behrle, T. L. Nguyen, F. Reiter, D. Baur, B. de Neeve, M. Stadler, M. Marinelli, F. Lancellotti, S. F. Yelin, and J. P. Home, Phonon laser in the quantum regime, Phys. Rev. Lett. **131**, 043605 (2023).
[21] P. C. Haljan, K.-A. Brickman, L. Deslauriers, P. J. Lee, and C. Monroe, Spin-dependent forces on trapped ions for phase-stable quantum gates and entangled states of spin and motion, Phys. Rev. Lett. **94**, 153602 (2005).
[22] F. Schmidt-Kaler, T. Feldker, D. Kolbe, J. Walz, M. Müller, P. Zoller, W. Li, and I. Lesanovsky, Rydberg excitation of trapped cold ions: a detailed case study, New J. Phys. **13**, 075014 (2011).
[23] T. Feldker, P. Bachor, M. Stappel, D. Kolbe, R. Gerritsma, J. Walz, and F. Schmidt-Kaler, Rydberg excitation of a single trapped ion, Phys. Rev. Lett. **115**, 173001 (2015).
[24] H. Labuhn, D. Barredo, S. Ravets, S. de Léséleuc, T. Macrì, T. Lahaye, and A. Browaeys, Tunable two-

dimensional arrays of single Rydberg atoms for realizing quantum Ising models, Nature **534**, 667 (2016).
[25] G. Higgins, W. Li, F. Pokorny, C. Zhang, F. Kress, C. Maier, J. Haag, Q. Bodart, I. Lesanovsky, and M. Hennrich, Single strontium Rydberg ion confined in a Paul trap, Phys. Rev. X **7**, 021038 (2017).
[26] A. Mokhberi, M. Hennrich, and F. Schmidt-Kaler, Trapped Rydberg ions: a new platform for quantum information processing (Academic Press, 2020) Chap. 4, pp. 233–306.
[27] M. Müller, L. Liang, I. Lesanovsky, and P. Zoller, Trapped Rydberg ions: from spin chains to fast quantum gates, New J. Phys. **10**, 093009 (2008).
[28] C. Zhang, F. Pokorny, W. Li, G. Higgins, A. Pöschl, I. Lesanovsky, and M. Hennrich, Submicrosecond entangling gate between trapped ions via Rydberg interaction, Nature **580**, 345 (2020).
[29] Z. Zhang, M. Yuan, B. Sundar, and K. R. A. Hazzard, Motional decoherence in ultracold Rydberg atom quantum simulators of spin models (2022), arXiv:2201.08463 [cond-mat.quant-gas].
[30] V. Bharti, S. Sugawa, M. Kunimi, V. S. Chauhan, T. P. Mahesh, M. Mizoguchi, T. Matsubara, T. Tomita, S. de Léséleuc, and K. Ohmori, Strong spin-motion coupling in the ultrafast quantum many-body dynamics of Rydberg atoms in a Mott-insulator lattice (2023), arXiv:2311.15575 [physics.atom-ph].
[31] F. M. Gambetta, C. Zhang, M. Hennrich, I. Lesanovsky, and W. Li, Long-range multibody interactions and three-body antiblockade in a trapped Rydberg ion chain, Phys. Rev. Lett. **125**, 133602 (2020).
[32] F. M. Gambetta, C. Zhang, M. Hennrich, I. Lesanovsky, and W. Li, Exploring the many-body dynamics near a conical intersection with trapped Rydberg ions, Phys. Rev. Lett. **126**, 233404 (2021).
[33] M. Magoni, R. Joshi, and I. Lesanovsky, Molecular dynamics in Rydberg tweezer arrays: spin-phonon entanglement and Jahn-Teller effect, Phys. Rev. Lett. **131**, 093002 (2023).
[34] M. Magoni, P. P. Mazza, and I. Lesanovsky, Emergent Bloch oscillations in a kinetically constrained Rydberg spin lattice, Phys. Rev. Lett. **126**, 103002 (2021).
[35] M. Magoni, P. P. Mazza, and I. Lesanovsky, Phonon dressing of a facilitated one-dimensional Rydberg lattice gas, SciPost Phys. Core **5**, 041 (2022).
[36] T. Amthor, C. Giese, C. S. Hofmann, and M. Weidemüller, Evidence of antiblockade in an ultracold Rydberg gas, Phys. Rev. Lett. **104**, 013001 (2010).
[37] C. Simonelli, M. M. Valado, G. Masella, L. Asteria, E. Arimondo, D. Ciampini, and O. Morsch, Seeded excitation avalanches in off-resonantly driven Rydberg gases, J. Phys. B **49**, 154002 (2016).
[38] F. Letscher, O. Thomas, T. Niederprüm, M. Fleischhauer, and H. Ott, Bistability versus metastability in driven dissipative Rydberg gases, Phys. Rev. X **7**, 021020 (2017).
[39] S. Helmrich, A. Arias, G. Lochead, T. Wintermantel, M. Buchhold, S. Diehl, and S. Whitlock, Signatures of self-organized criticality in an ultracold atomic gas, Nature **577**, 481 (2020).
[40] P. Kitson, T. Haug, A. La Magna, O. Morsch, and L. Amico, Rydberg atomtronic devices (2023), arXiv:2310.18242 [quant-ph].
[41] D. Brady and M. Fleischhauer, Mean-field approach to Rydberg facilitation in a gas of atoms at high and low temperatures (2023), arXiv:2308.14408 [cond-mat.quant-gas].
[42] Q. Xie, H. Zhong, M. T. Batchelor, and C. Lee, The quantum Rabi model: solution and dynamics, J. Phys. A **50**, 113001 (2017).
[43] S. Rinaldi, F. Melaccio, S. Gozem, F. Fanelli, and M. Olivucci, Comparison of the isomerization mechanisms of human melanopsin and invertebrate and vertebrate rhodopsins, Proc. Natl. Acad. Sci. U.S.A. **111**, 1714 (2014).
[44] C. Hempel, C. Maier, J. Romero, J. McClean, T. Monz, H. Shen, P. Jurcevic, B. P. Lanyon, P. Love, R. Babbush, A. Aspuru-Guzik, R. Blatt, and C. F. Roos, Quantum chemistry calculations on a trapped-ion quantum simulator, Phys. Rev. X **8**, 031022 (2018).
[45] F. Schlawin, M. Gessner, A. Buchleitner, T. Schätz, and S. S. Skourtis, Continuously parametrized quantum simulation of molecular electron-transfer reactions, PRX Quantum **2**, 010314 (2021).
[46] M. Han, J. Fedyk, J.-B. Ji, V. Despré, A. I. Kuleff, and H. J. Wörner, Observation of nuclear wave-packet interference in ultrafast interatomic energy transfer, Phys. Rev. Lett. **130**, 253202 (2023).
[47] R. J. MacDonell, T. Navickas, T. F. Wohlers-Reichel, C. H. Valahu, A. D. Rao, M. J. Millican, M. A. Currington, M. J. Biercuk, T. R. Tan, C. Hempel, and I. Kassal, Predicting molecular vibronic spectra using time-domain analog quantum simulation, Chem. Sci. **14**, 9439 (2023).
[48] J. Whitlow, Z. Jia, Y. Wang, C. Fang, J. Kim, and K. R. Brown, Quantum simulation of conical intersections using trapped ions, Nature Chem. **15**, 1509 (2023).
[49] C. H. Valahu, V. C. Olaya-Agudelo, R. J. MacDonell, T. Navickas, A. D. Rao, M. J. Millican, J. B. Pérez-Sánchez, J. Yuen-Zhou, M. J. Biercuk, C. Hempel, *et al.*, Direct observation of geometric-phase interference in dynamics around a conical intersection, Nature Chem. **15**, 1503 (2023).
[50] M. T. Djerad, Atomic parameters for transitions involving Rydberg states of singly ionized alkaline earths, J. Phys. II **1**, 1 (1991).
[51] See Supplemental Material at [URL] for a detailed derivation of the spin-phonon coupled model Hamiltonian and values for experimental and theoretical parameters, which additionally includes Refs. [58–84].
[52] W. Li and I. Lesanovsky, Electronically excited cold ion crystals, Phys. Rev. Lett. **108**, 023003 (2012).
[53] J. Vogel, W. Li, A. Mokhberi, I. Lesanovsky, and F. Schmidt-Kaler, Shuttling of Rydberg ions for fast entangling operations, Phys. Rev. Lett. **123**, 153603 (2019).
[54] F. Pokorny, C. Zhang, G. Higgins, and M. Hennrich, Magic trapping of a Rydberg ion with a diminished static polarizability (2020), arXiv:2005.12422 [physics.atom-ph].
[55] P. P. Mazza, R. Schmidt, and I. Lesanovsky, Vibrational dressing in kinetically constrained Rydberg spin systems, Phys. Rev. Lett. **125**, 033602 (2020).
[56] D. F. V. James, Quantum dynamics of cold trapped ions with application to quantum computation, Appl. Phys. B **66**, 181 (1998).
[57] J. W. P. Wilkinson, W. Li, and I. Lesanovsky, Code for "Spectral signatures of vibronic coupling in trapped cold atomic Rydberg systems" (2024).
[58] T. F. Gallagher, Rydberg atoms, Rep. Prog. Phys. **51**,

143 (1988).
[59] T. F. Gallagher, *Rydberg Atoms*, 1st ed. (Cambridge University Press, 1994).
[60] T. F. Gallagher, Rydberg atoms, in *Springer Handbook of Atomic, Molecular, and Optical Physics*, edited by G. W. F. Drake (Springer, 2023) Chap. 15.
[61] W. Paul, Electromagnetic traps for charged and neutral particles, Rev. Mod. Phys. **62**, 531 (1990).
[62] D. J. Wineland, C. Monroe, W. M. Itano, D. Leibfried, B. E. King, and D. M. Meekhof, Experimental issues in coherent quantum-state manipulation of trapped atomic ions, J. Res. Natl. Inst. Stand. Technol. **103**, 259 (1998).
[63] D. Leibfried, R. Blatt, C. Monroe, and D. J. Wineland, Quantum dynamics of single trapped ions, Rev. Mod. Phys. **75**, 281 (2003).
[64] F. G. Major, V. N. Gheorghe, and G. Werth, *Charged Particle Traps*, 1st ed. (Springer, 2005).
[65] D. Hucul, M. Yeo, S. Olmschenk, C. Monroe, W. K. Hensinger, and J. Rabchuk, On the transport of atomic ions in linear and multidimensional ion trap arrays, Quant. Inf. Comput. **8**, 501 (2008).
[66] C. F. Foot, *Atomic Physics*, 1st ed. (Oxford University Press, 2004).
[67] M. Aymar, C. H. Greene, and E. Luc-Koenig, Multichannel Rydberg spectroscopy of complex atoms, Rev. Mod. Phys. **68**, 1015 (1996).
[68] D. J. Berkland, J. D. Miller, J. C. Bergquist, W. M. Itano, and D. J. Wineland, Minimization of ion micromotion in a Paul trap, J. Appl. Phys. **83**, 5025 (1998).
[69] R. J. Cook, D. G. Shankland, and A. L. Wells, Quantum theory of particle motion in a rapidly oscillating field, Phys. Rev. A **31**, 564 (1985).
[70] D. J. Griffiths, *Introduction to Electrodynamics*, 4th ed. (Cambridge University Press, 2017).
[71] D. J. Griffiths and D. F. Schroeter, *Introduction to Quantum Mechanics*, 3rd ed. (Cambridge University Press, 2018).
[72] H. Friedrich, *Theoretical Atomic Physics*, 4th ed. (Springer, 2017).
[73] M. Saffman, T. G. Walker, and K. Mølmer, Quantum information with Rydberg atoms, Rev. Mod. Phys. **82**, 2313 (2010).
[74] J. J. Bollinger, D. J. Wineland, and D. H. E. Dubin, Non-neutral ion plasmas and crystals, laser cooling, and atomic clocks, Phys. Plasmas **1**, 1403 (1994).
[75] D. G. Enzer, M. M. Schauer, J. J. Gomez, M. S. Gulley, M. H. Holzscheiter, P. G. Kwiat, S. K. Lamoreaux, C. G. Peterson, V. D. Sandberg, D. Tupa, A. G. White, R. J. Hughes, and D. F. V. James, Observation of power-law scaling for phase transitions in linear trapped ion crystals, Phys. Rev. Lett. **85**, 2466 (2000).
[76] S. Fishman, G. De Chiara, T. Calarco, and G. Morigi, Structural phase transitions in low-dimensional ion crystals, Phys. Rev. B **77**, 064111 (2008).
[77] A. Kleczewski, M. R. Hoffman, J. A. Sherman, E. Magnuson, B. B. Blinov, and E. N. Fortson, Coherent excitation of the $6S_{1/2}$ to $5D_{3/2}$ electric-quadrupole transition in $^{138}Ba^{+}$, Phys. Rev. A **85**, 043418 (2012).
[78] S. R. Williams, A. Jayakumar, M. R. Hoffman, B. B. Blinov, and E. N. Fortson, Method for measuring the $6S_{1/2} \leftrightarrow 5D_{3/2}$ magnetic-dipole-transition moment in Ba^{+}, Phys. Rev. A **88**, 012515 (2013).
[79] I. V. Inlek, C. Crocker, M. Lichtman, K. Sosnova, and C. Monroe, Multispecies trapped-ion node for quantum networking, Phys. Rev. Lett. **118**, 250502 (2017).
[80] D. Kolbe, M. Scheid, and J. Walz, Triple resonant four-wave mixing boosts the yield of continuous coherent vacuum ultraviolet generation, Phys. Rev. Lett. **109**, 063901 (2012).
[81] P. Bachor, T. Feldker, J. Walz, and F. Schmidt-Kaler, Addressing single trapped ions for Rydberg quantum logic, J. Phys. B: At. Mol. Opt. Phys. **49**, 154004 (2016).
[82] S. Weber, C. Tresp, H. Menke, A. Urvoy, O. Firstenberg, H. P. Büchler, and S. Hofferberth, Calculation of Rydberg interaction potentials, J. Phys. B: At. Mol. Opt. Phys. **50**, 133001 (2017).
[83] J. D. Louck, Angular Momentum Theory, in *Springer Handbook of Atomic, Molecular, and Optical Physics*, edited by G. W. F. Drake (Springer, 2023) Chap. 2.
[84] W. Li, A. W. Glaetzle, R. Nath, and I. Lesanovsky, Parallel execution of quantum gates in a long linear ion chain via Rydberg mode shaping, Phys. Rev. A **87**, 052304 (2013).